Reliability Assessment of Diaphragm Wall Deflections in Soft Clays

Anthony T.C. Goh[1], Feng Xuan[2] and Wengang Zhang[3]

[1]Associate Professor, School of Civil & Environmental Engrg., Nanyang Technological University, Nanyang Avenue, Singapore 639798. ctcgoh@ntu.edu.sg
[2]former Graduate Student, School of Civil & Environmental Engrg., Nanyang Technological University, Nanyang Avenue, Singapore 639798. fox110710@163.com
[3]Research Associate, School of Civil & Environmental Engrg., Nanyang Technological University, Nanyang Avenue, Singapore 639798. zhangwg@ntu.edu.sg

ABSTRACT: For excavations in built-up areas with deep deposits of soft clays, it is essential to control ground movements to minimize damage to adjacent structures and facilities. This is commonly carried out by controlling the deflections of the retaining wall system. The limiting wall deflection or serviceability limit state is typically taken to be a percentage of the excavation height. In this study, extensive plane strain finite element analyses have been carried out to examine the excavation-induced wall deflections for a deep deposit of soft clay supported by diaphragm walls and bracing. Based on the numerical results, two polynomial regression approaches were used to develop the equations for estimating the maximum wall deflection. This paper describes how the developed equations can be used to perform reliability analysis of the diaphragm wall serviceability limit state to estimate the probability of exceeding the limiting wall deflection.

INTRODUCTION

In many urban environments the underlying soil comprises of thick soft clays overlying stiff clay. For excavation in these soil conditions, diaphragm walls are often used to minimize ground movements and damage to adjacent structures. The limiting wall deflection is typically taken to be a percentage of the excavation height. To prevent basal heave failure and to reduce the movement of the wall toe, extending the wall length into the stiff clay layer is commonly carried out. To date, many empirical methods (e.g., Mana & Clough 1981; Wong & Broms 1989; Clough & O'Rourke 1990) have been proposed for estimating wall movements. These studies have demonstrated that the major factors affecting the excavation performance include: excavation width and depth, wall stiffness, strut spacing, stiffness and preloading, depth to an underlying hard stratum, soil stiffness and strength distribution, adjacent surcharge and quality of workmanship. In general, these methods assume that the wall (either a flexible sheet pile wall or a stiff concrete wall) is "floating" in the soft clay, without restraint at the wall toe. This paper focuses on the specific situation of the diaphragm wall penetrating into the stiff stratum.

For excavations in soft clays, the Mohr-Coulomb constitutive relationship is commonly used to model the clay stress-strain behavior, with no consideration of the soil small strain effect. The importance of modeling the soil small strain behavior for many geotechnical problems has been highlighted by Burland (1989) and Jardine et al. (1986). The influence of the soil small strain effect on excavation problems which has been investigated through finite element analysis with some advanced small strain constitutive models (e.g., Benz 2007; Kung et al. 2009) showed improvements in the predictions of wall deflection and ground movement.

In this paper, plane strain finite element analyses using Plaxis (Brinkgreve et al. 2006) were performed in which the soft clay stress-strain behavior was modeled using the hardening small strain (HSS) constitutive relationship that considers the small strain effect. Parametric studies were carried out to evaluate the behavior of excavations with diaphragm walls in soft clay. Based on these results, this paper describes simplified regression equations that were developed for estimating the maximum wall deflection and demonstrates how to perform reliability analysis of

the diaphragm wall serviceability limit state to estimate the probability of the wall deflection exceeding the limiting wall deflection.

SOIL MODEL

The hardening-soil (HS) model (Schanz et al. 1999) is an advanced constitutive soil model for simulating the behavior of soils. The model involves frictional hardening characteristics to model plastic shear strain in deviatoric loading, and cap hardening to model plastic volumetric strain in primary compression. Failure is defined by the Mohr-Coulomb failure criterion. The main input parameters are E_{50}^{ref}, a reference secant modulus corresponding to the reference confining pressure p^{ref}, a power m for stress-dependent stiffness formulation, effective friction angle ϕ, cohesion c, failure ratio R_f, E_{ur}^{ref} the reference stiffness modulus for unloading and reloading corresponding to the reference pressure p^{ref}, and υ_{ur} the unloading and reloading Poisson's ratio.

The HSS model is based on the HS model with two additional small strain parameters: G_0^{ref} a reference initial shear stiffness corresponding to the reference pressure and shear strain $\gamma_{0.7}$ at which the secant shear modulus is reduced to 70% of G_0. The value $\gamma_{0.7} = 2x10^{-4}$ was assumed in all the analyses.

In order to study the influence of the shear strength of the soft clay, a series of analysis were carried out using the HSS model in which the soil shear strength ratio c_u/σ'_v ratio was varied where c_u is the undrained shear strength and σ'_v is the vertical effective stress. For an assumed c_u/σ'_v ratio, the effective friction angle ϕ is computed using the correlation proposed by Wroth and Houlsby (1985):

$$\frac{c_u}{\sigma'_v} = 0.5743\frac{3\sin\phi}{3-\sin\phi} \tag{1}$$

The Plaxis default values are used to define the power for stress-level dependency of the stiffness m, the coefficient of earth pressure at-rest K_0^{nc}, the Poisson's ratio υ_{ur} and E_{ur} with m = 1, $K_0^{nc} = 1 - \sin\phi$, $\upsilon_{ur} = 0.2$ and $E_{ur} = 3E_{50}$.

FINITE ELEMENT ANALYSES

Parametric studies have been carried out using the HSS model for the soft clay with emphasis on the maximum wall deflection predictions. Figure 1 shows the geometry of the hypothetical case considered, and is typical of a soil profile in coastal areas with stiff clay layer underlying the thick normally consolidated soft clay layer. The Mohr Coulomb constitutive relationship was used to model the stiff clay ($\gamma = 20$ kN/m^3, $c_u = 500$ kPa, $E_u = 250$ MPa). The soft clay thickness is denoted as T in Figure 1.

The analyses considered a plane strain excavation supported by a diaphragm wall. Because of symmetry, only half the cross-section was considered. The soil was modeled by 15-noded triangular elements. The structural elements were assumed to be linear elastic with the wall represented by 5-noded beam elements and 3-noded bar elements were used for the 7 levels of struts located at depths of 2 m, 5 m, 8 m, 11 m, 14 m and 17 m below the original ground surface. The nodes along the side boundaries of the mesh were constrained from displacing horizontally while the nodes along the bottom boundary were constrained from moving horizontally and vertically. The range of properties that were varied are shown in Table 1. This study only considered the use of diaphragm walls.

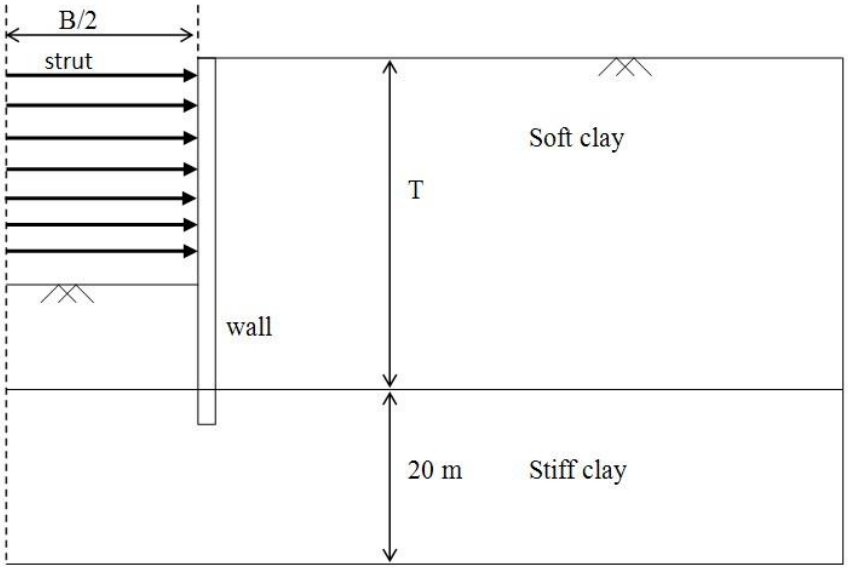

Figure 1. Cross-sectional soil and wall profile.

The construction sequence comprised the following steps: (1) the wall is installed ("wished into place") without any disturbance in the surrounding soil; (2) the soil is excavated uniformly 1 m below each strut level prior to adding the strut support with struts at 3 m vertical spacings until the final depth H_e of 20 m is reached. The soil is assumed to be subjected to undrained shearing during excavation. For simplicity, for most of the cases presented, the groundwater table is assumed to be at the original ground surface with hydrostatic pore pressure conditions. The influence of the groundwater table is described later.

For brevity only some general trends observed as various parameters were varied are presented. The influence of soil stiffness ratio E_{50}/c_u is shown in Figure 2 for cases with γ = 17 kN/m^3, B = 30 m, c_u/σ'_v = 0.29 and T = 30 m. The influence of E_{50}/c_u is more significant for lower wall thickness d. The influence of the soil shear strength ratio c_u/σ'_v for the cases with γ = 17 kN/m^3, B = 40 m, d = 0.9 m, E_{50}/c_u = 200 and T = 30 m is presented in Figure 3. The results show the maximum wall deflection decreases with the increase of soil shear strength ratio.

Table 1. Range of parameters.

Parameter	Range
Soil shear strength ratio c_u/σ'_v	0.21, 0.25, 0.29, 0.34
Soil stiffness ratio E_{50}/c_u	100, 200, 300
Soil unit weight γ (kN/m^3)	15, 17, 19
Soft clay thickness T (m)	25, 30, 35
Excavation width B (m)	20, 30, 40, 50, 60
Excavation depth h (m)	8, 11, 14, 17, 20
Strut stiffness EA ($\times 10^5$ kN/m)	2.5, 5, 10, 15, 30
Wall thickness d (m)	0.6, 0.9, 1.2, 1.5
Wall stiffness EI ($\times 10^6$ kNm^2/m)	0.36, 1.21, 2.88, 5.63

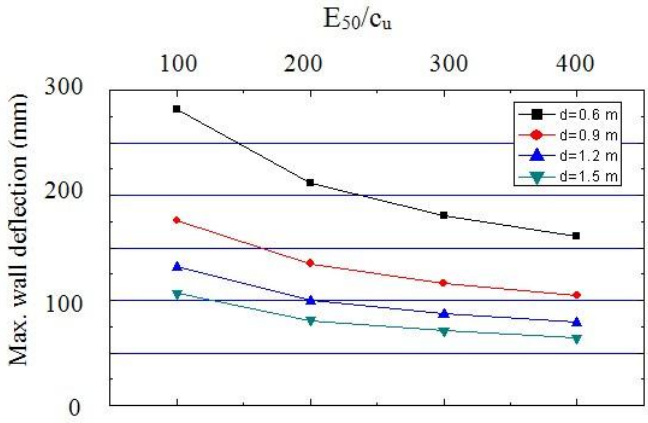

Figure 2. Effect of soil stiffness on wall deflection for h = 20 m.

The excavation strutting system is one of the structural components affecting the wall deflection. In this study, the vertical strut spacing h_{avg} is assumed to be 3 m as is common in many excavation sites. The effect of strut stiffness is illustrated in Figure 4 for a series of analyses with γ = 17 kN/m^3, B = 40 m, h = 20 m, c_u/σ'_v = 0.29, E_{50}/c_u, = 200 and T = 30 m. The results show that the deflection ratio μ_S (which is defined as the maximum wall deflection divided by the maximum wall deflection for the case with strut stiffness EA = 1.0x10^6 kN/m) decreases with increasing strut stiffness, but the effect is not very significant when the strut stiffness EA exceeds 1.5x10^6 kN/m. The results also show that for concrete diaphragm walls the influence of the wall stiffness (represented by the wall thickness d) is minimal. The factor μ_S will be used later in the proposed simplified mathematical equation to estimate wall deflections.

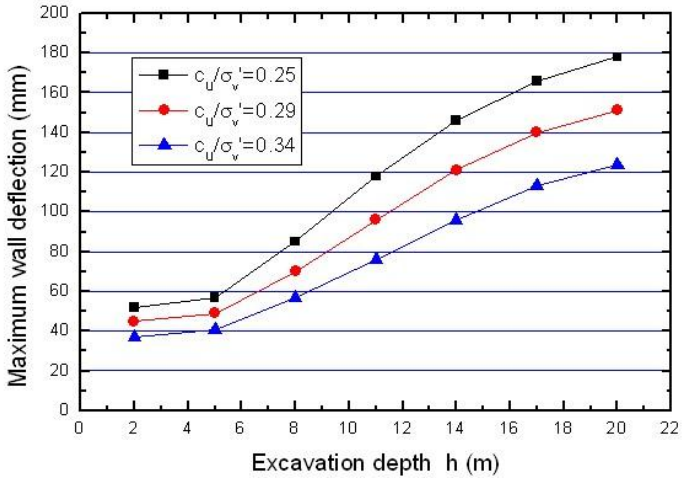

Figure 3. Effect of soil shear strength ratio on wall deflection for d = 0.9 m.

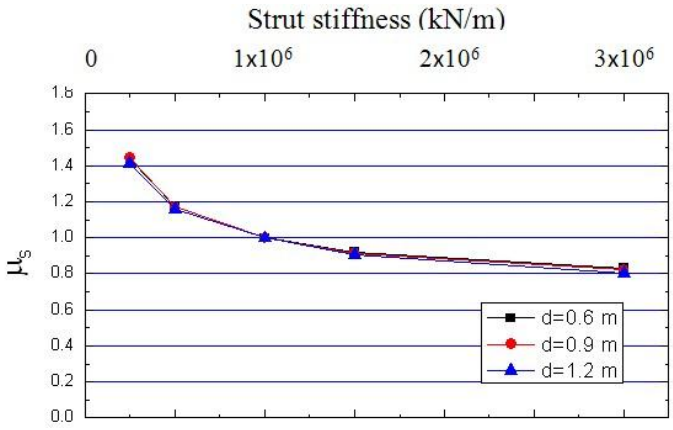

Figure 4. Plot of μ_S versus strut stiffness.

In the previous analyses, the groundwater table was assumed at the ground surface, which is the most unfavorable condition. In many situations with soft clay, the groundwater table could be 1 to 2 m below the ground surface. To study the influence of the groundwater table, a series of analyses were carried out assuming various groundwater levels. Defining the deflection ratio μ_W as the maximum wall deflection divided by the maximum wall deflection for the case where the groundwater table is at the ground surface, the results indicate that μ_W decreases almost linearly with decreasing groundwater level. The factor μ_W can be estimated as $\mu_W = 1 - 0.1l$, where l is the depth of the ground water table below the ground surface (in metres) and $l \leq 2$ m. The factor μ_W will be used later in the proposed simplified mathematical equations to estimate wall deflections.

DETERMINATION OF RESPONSE SURFACE

In order to carry out reliability analysis of the diaphragm wall serviceability limit state to estimate the probability of the wall deflection exceeding the limiting wall deflection, the failure domain response surface first needs to be determined. Because of the complexity of modeling this highly nonlinear problem involving a large number of variables, the serviceability failure domain was constructed artificially through repeated point-by-point numerical analyses. A total of 1120 cases were analyzed (Xuan 2009) for the maximum diaphragm wall deflection. The ranges of the variables are shown in Table 1. Various different techniques to model the response surface have been proposed including artificial neural networks (Goh and Kulhawy 2005) and regression methods (Kung et al. 2007). In this paper, two different approaches were considered for developing the response surface equation. In the first approach, regression analysis using a trial-and-error process was used to develop the explicit function for the maximum wall deflection δ_{h0} as a function of seven input parameters: the soil unit weight γ, the excavation width B, the excavation depth h, the soil shear strength ratio c_u/σ'_v, the soil stiffness ratio E_{50}/c_u, the system stiffness $EI/\gamma_w h_{avg}^4$, and the soft clay thickness T. The term h_{avg} refers to the average vertical spacing of the struts. The regression equation for wall deflection takes the following form:

$$\delta_{h0} = a_0 + a_1 B + a_2 B^2 + a_3 T + a_4 T^2 + a_5 h + a_6 h^2 + a_7 (c_u/\sigma'_v) + a_8 (c_u/\sigma'_v)^2 +$$
$$a_9 \left(\frac{E_{50}}{c_u}\right) + a_{10} \left(\frac{E_{50}}{c_u}\right)^2 + a_{11} \ln(EI/\gamma_w h_{avg}^4) + a_{12} \ln^2(EI/\gamma_w h_{avg}^4) +$$
$$a_{13}\gamma + a_{14}\gamma^2 + a_{15} h.\ln(EI/\gamma_w h_{avg}^4) \qquad (2)$$

The values of the coefficients are shown in Table 2. A comparison of the maximum wall deflection values computed using (2) versus the predicted values from the finite element analyses for all the cases indicated a fairly high accuracy with a coefficient of determination R^2 of 0.88.

The second approach involved the use of a simple nonparametric regression algorithm known as multivariate adaptive regression splines (MARS) to model the nonlinear interactions between variables (Friedman 1991). The MARS method makes no specific assumption about the underlying functional relationship between the input variables and the response. The main advantages of MARS are its capacity to produce simple, easy-to-interpret models, its ability to estimate the contributions of the input variables, and its computational efficiency. The underlying idea behind MARS is to allow potentially different linear or nonlinear polynomial functions over different intervals. The end points of the intervals are called knots. A knot marks the end of one region of data and the beginning of another. The resulting piecewise curve (spline), gives greater flexibly to the model, allowing for bends and other departures from linear functions. An adaptive regression algorithm is used for selecting the knot locations. MARS models are constructed in a two-phase procedure. The first (forward) phase adds functions and finds potential knots to improve the performance, resulting in an overfit model. The second (backward) phase involves pruning the least effective terms using a Generalized Cross-Validation method that penalize large numbers of basis functions BFs and serves to reduce the chance of overfitting.

Table 2. Response surface coefficient for δ_{h0}.

a_0	1612.23	a_4	-0.0456	a_8	699.08	a_{12}	8.78
a_1	2.524	a_5	38.76	a_9	-0.881	a_{13}	-118.05
a_2	-0.0169	a_6	-0.256	a_{10}	0.00131	a_{14}	2.978
a_3	7.55	a_7	-1014.39	a_{11}	-119.04	a_{15}	-3.31

The MARS model $f(X)$ is constructed as a linear combination of splines (also known as basis functions BFs) and their interactions, and is expressed as:

$$f(X) = \beta_0 + \sum_{m=1}^{M} \beta_m \lambda_m(X) \tag{3}$$

where each λ_m is a basis function. It can be a spline function, or the product of two or more spline functions already contained in the model (higher orders can be used when the data warrants it; for simplicity, at most second order is assumed in this paper). The coefficients β_i are constants, estimated using the least-squares method.

For the analysis, the same database used to formulate (2) was divided into 840 training patterns and 280 testing (validation) patterns. The optimal MARS model consisted of 22 BFs of linear spline functions with second-order interaction. Execution time of 1.11 seconds indicates the computational efficiency of MARS. The coefficient of determination R^2 values of 0.938 and 0.949 for the training and testing patterns respectively indicate that the MARS model is another alternative to (2) that can also be used. Table 3 lists the BFs and their corresponding equations for the optimal MARS model. The term max in Table 3 can be explained as: max (a, b) is equal to a if a > b, else b. The interpretable MARS model in the format of linear combination of BFs as shown in (3) is given by

$$\begin{aligned}\delta_{h0} = {} & 165 - 50.889*BF1 + 66.598*BF2 - 0.1914*BF3 + 0.4956*BF4 - 10.324*BF5 + 19.135*BF6 - \\ & 326.34*BF7 + 815.69*BF8 + 4.9881*BF9 - 6.1891*BF10 + 7.4897*BF11 - 7.0073*BF12 \\ & -13.712*BF13 + 24.131*BF14 + 540.93*BF15 - 331.28*BF16 + 2.7716*BF17 \\ & - 4.5821*BF18 -1.1808*BF19 + 0.8612*BF20 + 0.5114*BF21 - 1.5474*BF22 \end{aligned} \tag{4}$$

Table 3. Basis functions and their corresponding equations for δ_{h0}.

Basis Function	Equation
BF1	$\max(0, \ln(EI/\gamma_w h_{avg}^4) - 7.313)$
BF2	$\max(0, 7.313 - \ln(EI/\gamma_w h_{avg}^4))$
BF3	$\max(0, E_{50}/c_u - 200)$
BF4	$\max(0, 200 - E_{50}/c_u)$
BF5	$\max(0, \gamma - 17)$
BF6	$\max(0, 17 - \gamma)$
BF7	$\max(0, c_u/\sigma'_v - 0.25)$
BF8	$\max(0, 0.25 - c_u/\sigma'_v)$
BF9	$\max(0, h - 17)$
BF10	$\max(0, 17 - h)$
BF11	$\max(0, T - 30)$
BF12	$\max(0, 30 - T)$
BF13	BF6 * $\max(0, \ln(EI/\gamma_w h_{avg}^4) - 7.313)$
BF14	BF6 * $\max(0, 7.313 - \ln(EI/\gamma_w h_{avg}^4))$
BF15	BF7 * $\max(0, \ln(EI/\gamma_w h_{avg}^4) - 8.176)$
BF16	BF7 * $\max(0, 8.176 - \ln(EI/\gamma_w h_{avg}^4))$
BF17	BF10 * $\max(0, \ln(EI/\gamma_w h_{avg}^4) - 7.313)$
BF18	BF10 * $\max(0, 7.313 - \ln(EI/\gamma_w h_{avg}^4))$
BF19	BF10 * $\max(0, T - 30)$
BF20	BF10 * $\max(0, 30 - T)$
BF21	$\max(0, B - 40)$
BF22	$\max(0, 40 - B)$

For either (2) or (4), corrections for the depth of the groundwater table (described in the previous section) and strut stiffness can be considered using:

$$\delta_{hm} = \mu_w \mu_s \delta_{h0} \tag{5}$$

where μ_w is the correction factor for water table, and μ_s is the correction for strut stiffness (Figure 4). Predictions using (2) and (5) were found to compare well with measured results from a number of documented case studies (Xuan 2009).

RELIABILITY ANALYSIS

With the determination of the response surface equations (2) and (4) as outlined in the previous section, reliability assessment of the diaphragm wall serviceability limit state can be carried out using a spreadsheet algorithm (Goh and Kulhawy 2005) as described in the following. The reliability index β using the first order reliability method (FORM) proposed by Hasofer and Lind (1974) can be determined using:

$$\beta = \min_{X \in F} \sqrt{\left[\frac{x - m}{\sigma}\right]^T [R]^{-1} \left[\frac{x - m}{\sigma}\right]} \tag{6}$$

where x = vector of random variables; m = vector of mean values; σ = vector of standard deviation;

R = correlation matrix; and F = failure region.

For the illustrative case shown in Table 4, the reliability analysis spreadsheet for normally distributed and uncorrelated variables is shown in Figure 5. For illustration, the predicted maximum wall deflection derived from (2) and (5) is 75 mm. The limiting wall deflection is 87.5 mm or 175 mm when $\delta_{h,lim}$ of 0.5% or 1% of the excavation height H_e is adopted. The step-by-step procedure for setting up Figure 5 is described in the following:

1. Input the mean values (D5:D20) to calculate the predicted maximum wall deflection (F21). Modify with μ_w (D22) and μ_s (D23) to obtain δ_{hm} (F24).
2. Input the mean value in 'x value' (I5:I13) and 'mean' (J5:J13), and transpose 'x value' as $[X']^T$ (C31:R31) which coincides with the response surface coefficient column (E5:E20). Input COV in (L5:L13) and obtain σ in (K5:K13), as well as the column [nx] in (M5:M13) which contains the equation $(x_i - \mu_i)/\sigma_i$. Transpose (built-in spreadsheet function) [nx] in (C28:K28).
3. Input the element matrix R, inverse (built-in spreadsheet function) R to obtain $[R]^{-1}$.
4. Invoke the 'Solver' option in the spreadsheet. Minimize reliability index β in (J16). Change 'x value' in (I5:I13). Constraint $g(x) = \delta_{h,lim} - \delta_{hm}$ in (J25), where $\delta_{h,lim} = 1.0\%$ or $0.5\%H_e$ and $\delta = (I12)(I13)[X']^T[E5:E20]$.
5. Obtain β and $P_f = 1 - NORMSDIST(\mu)$, where NORMSDIST is the spreadsheet function returning the standard normal cumulative distribution.

Table 4. Mean value and COV assumed for example.

Variable	Mean	COV	Variable	Mean	COV
c_u/σ_v'	0.285	15%	B (m)	21	5%
E_{50}/c_u	150	15%	T (m)	22	5%
γ (kN/m^3)	17.3	7%	h (m)	17.5	5%
$\ln(EI/\gamma_w h^4_{avg})$	7.3	1.9%	μ_w	0.8	5%
			μ_S	1.02	5%

Monte Carlo simulations (MCS) for the limiting wall deflection of $1.0\%H_e$ as shown in Table 5 indicate that the reliability index computed using FORM and MCS are comparable. The influence of the COV of c_u/σ'_v computed using (4) is presented in Figure 6 for the limiting wall deflection of $1.0\%H_e$. As expected, the P_f increases from approximately 1% to 20% when COV of c_u/σ'_v increases from 0.1 to 0.5.

RELIABILITY ANALYSIS

A parametric study using the hardening small strain constitutive soil model has been carried out to examine the behavior of diaphragm walls in soft clays overlying a stiffer stratum. The maximum wall deflection was found to be influenced by a number of factors: the excavation width and depth, the soft clay properties and thickness, the wall and strut properties, and the groundwater level. Based on the numerical results, two alternative mathematical equations were developed for predicting the maximum lateral wall displacement. Subsequently, based on the proposed response surface expressions, a spreadsheet was developed for performing reliability analysis of the serviceability limit state for diaphragm walls in soft clay. The proposed methodology is potentially useful for optimization of braced excavation design using diaphragm walls.

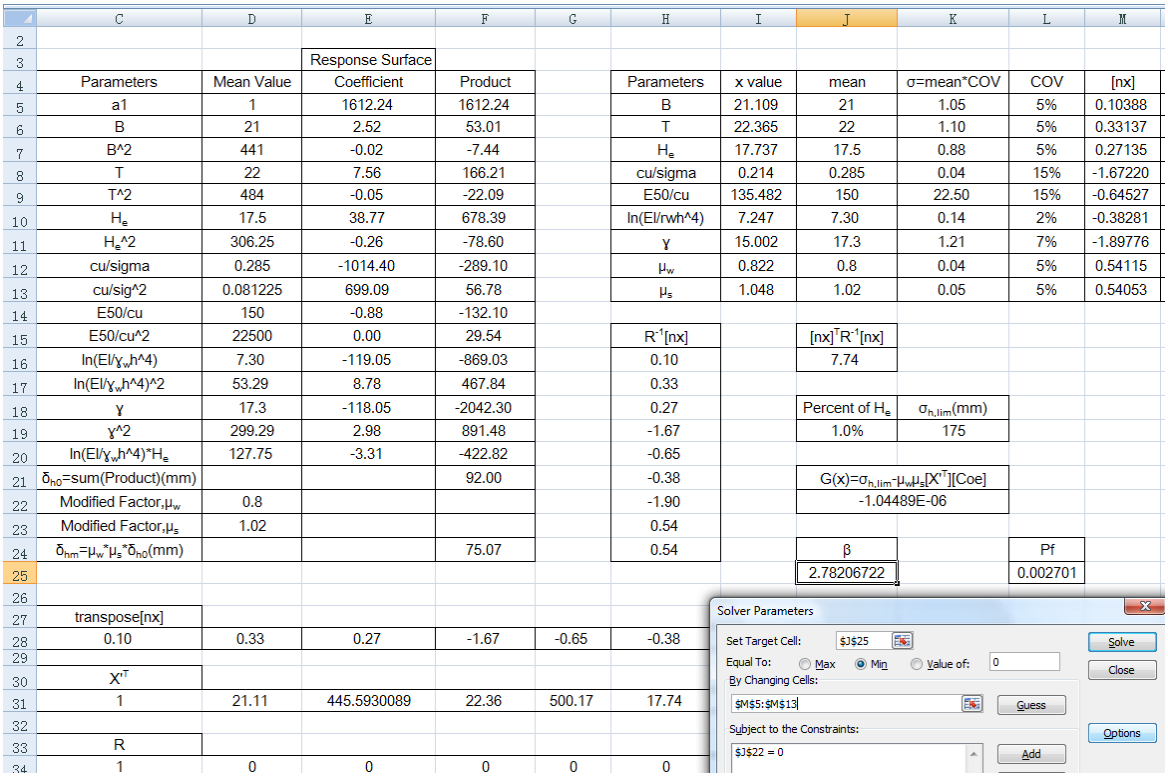

Parameters	Mean Value	Response Surface Coefficient	Product
a1	1	1612.24	1612.24
B	21	2.52	53.01
B^2	441	-0.02	-7.44
T	22	7.56	166.21
T^2	484	-0.05	-22.09
H_e	17.5	38.77	678.39
H_e^2	306.25	-0.26	-78.60
cu/sigma	0.285	-1014.40	-289.10
cu/sig^2	0.081225	699.09	56.78
E50/cu	150	-0.88	-132.10
E50/cu^2	22500	0.00	29.54
ln(El/$\gamma_w h$^4)	7.30	-119.05	-869.03
ln(El/$\gamma_w h$^4)^2	53.29	8.78	467.84
γ	17.3	-118.05	-2042.30
γ^2	299.29	2.98	891.48
ln(El/$\gamma_w h$^4)*H_e	127.75	-3.31	-422.82
δ_{h0}=sum(Product)(mm)			92.00
Modified Factor,μ_w	0.8		
Modified Factor,μ_s	1.02		
$\delta_{hm}=\mu_w*\mu_s*\delta_{h0}$(mm)			75.07

transpose[nx]					
0.10	0.33	0.27	-1.67	-0.65	-0.38

X'^T					
1	21.11	445.5930089	22.36	500.17	17.74

R					
1	0	0	0	0	0

Parameters	x value	mean	σ=mean*COV	COV	[nx]
B	21.109	21	1.05	5%	0.10388
T	22.365	22	1.10	5%	0.33137
H_e	17.737	17.5	0.88	5%	0.27135
cu/sigma	0.214	0.285	0.04	15%	-1.67220
E50/cu	135.482	150	22.50	15%	-0.64527
ln(El/rwh^4)	7.247	7.30	0.14	2%	-0.38281
γ	15.002	17.3	1.21	7%	-1.89776
μ_w	0.822	0.8	0.04	5%	0.54115
μ_s	1.048	1.02	0.05	5%	0.54053

R^{-1}[nx]	$[nx]^T R^{-1}$[nx]
0.10	7.74
0.33	
0.27	
-1.67	
-0.65	
-0.38	
-1.90	
0.54	
0.54	

Percent of H_e	$\sigma_{h,lim}$(mm)
1.0%	175

G(x)=$\sigma_{h,lim}-\mu_w\mu_s[X^T][Coe]$
-1.04489E-06

β	Pf
2.78206722	0.002701

Figure 5. Sample spreadsheet for performing reliability analysis.

Table 5. Summary of β for limiting wall deflection of 1.0%H_e.

	Equation (2)		Equation (4)	
	FORM	MCS	FORM	MCS
Reliability index β	2.51	1.98	2.20	2.14

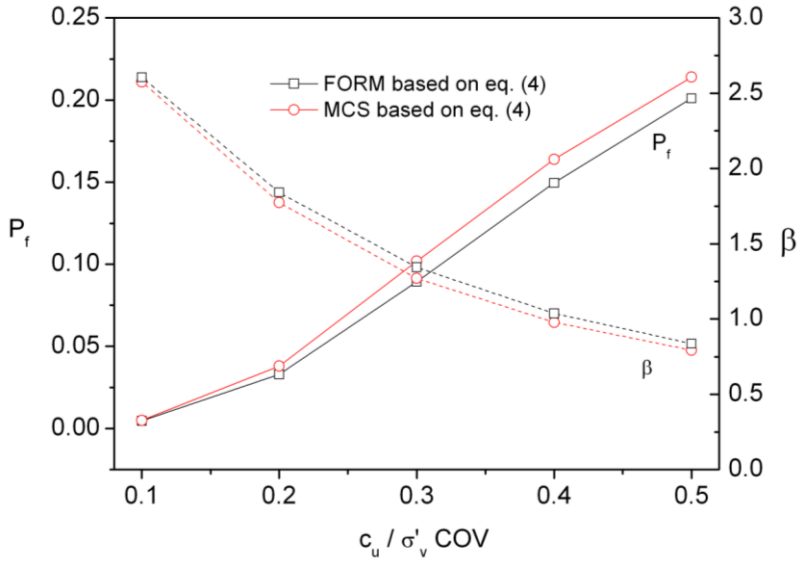

Figure 6. Influence of soil strength ratio on P_f.

ACKNOWLEDGMENTS

The authors appreciate the support of the Defense Science and Technology Agency Singapore for partially funding this research project.

REFERENCES

Benz, T. (2007). Small-strain stiffness of soil and its numerical consequences. Ph.D. Thesis, Univ. Stuttgart.

Brinkgreve, R.B.J, Broere, W. & Waterman, D. (2006). PLAXIS version 8.5 Manual. Rotterdam: A A Balkema.

Burland, J.B. (1989). "Small is beautiful - the stiffness of soils at small strains". *Canadian Geotechnical Journal*, 26 (4), 499–516.

Clough G.W. & O'Rourke, T.D. (1990). "Construction induced movements of in situ walls". *Design and Performance of Earth Retaining Structures*, ASCE Special Conference, Ithaca, New York, 439-470.

Friedman, J.H. (1991). Multivariate adaptive regression splines". *The Annals of Statistics*,19, 1-141.

Goh, A.T.C. & Kulhawy, F.H. (2005). "Reliability assessment of serviceability performance of braced retaining walls using a neural network approach". *International Journal for Numerical and Analytical Methods in Geomechanics*, 29 (6), 627-642.

Hasofer, A.M. & Lind, N.C. (1978). "Exact and invariant second moment code format". *Journal Engineering Mechanics Division*, ASCE, 100 (1), 111-121.

Jardine, R.J., Potts, D.M., Fourie, A.B. & Burland, J.B. (1986). "Studies of the influence of non-linear stress-strain characteristics in soil-structure interaction". *Géotechnique*, 36 (3), 377–396.

Kung, G.T.C., Juang, C.H., Hsiao, E.C. & Hashash, M.A. (2007). "Simplified Model for Wall Defelction and Ground-surface Settlement Caused by Braced Excavation in Clays", *Journal of Geotechnical and Geoenvironmental Engineering*, ASCE, 133 (6), 731-747.

Kung, G.T.C., Ou, C.Y. & Juang, C.H. (2009). "Modeling small-strain behavior of Taipei clays for finite element analysis of braced excavations". *Computers and Geotechnics*, 36 (1), 304-319.

Mana, A.I. & Clough, G.W. (1981). "Prediction of movement for braced cuts in clay". *Journal Geotechnical Engineering Division*, ASCE, 107 (6), 759-777.

Schanz, T., Vermeer, P.A. & Bonnier, P.G. (1999). "The hardening soil model-formulation and verification". *Beyond 2000 in Computational Geotechnics*. Amsterdam, A.A. Balkema, 281-296.

Wong, K.S. & Broms, B.B. (1989). "Lateral wall deflections of braced excavation in clay". *Journal of Geotechnical Engineering*, ASCE, 115 (6), 853-870.

Wroth, C.P. & Houlsby, G.T. (1985). "Soil mechanics-property characterization and analysis procedures". *11th International Conference on Soil Mechanics and Foundations Engineering*. San Francisco, 1985. 1: 1-55.

Xuan, F. (2009) Behavior of diaphragm walls in clays and reliability analysis. M.Eng. Thesis, Nanyang Technological University, Singapore.